Constraining the Irradiance of Point Reflectors in Conjugate Geometries: An Elementary Derivation

Matthew Phelps
United States Space Force, Space Systems Command (A&AS)
Justin Fletcher
United States Space Force, Space Systems Command (A&AS)

ABSTRACT

In this work, we derive a relation between the irradiance measured at the image plane of two conjugate sensor-target-source geometries. Such a relation is of interest in the application of ground-based optical sensors taking measurements of point-like geosynchronous space objects illuminated by the sun. The relation rests on a particular symmetry of the bidirectional reflectance distribution function (BRDF) known as Helmholtz reciprocity. Given the conjugate relation, we are able to directly relate the expected irradiance from a point reflector in one orientation to the expected irradiance in a conjugate orientation conditioned on a unique illumination geometry. Such a technique may enable one to match the optical spectra of a post-oriented geosynchronous space object to a registry of pre-oriented optical spectra at the conjugate geometry and thereby quantitatively infer the new orientation.

1. INTRODUCTION

To calculate the irradiance on a given surface arising from the reflections of a point-target illuminated by a spherical source, we make use of a few concepts of radiometry. First, we compute the irradiance from a Lambertian sphere arriving at the surface of the target. This incident irradiance is then used to compute the reflected outgoing radiance from the target in association with its bidirectional reflectance distribution function (BRDF). Finally, taking into account the entrance pupil size and focal length of a simple optical system, we calculate the irradiance incident on the image plane. We discuss the assumptions and approximations used to derive the simple reflection model. We also motivate a potential application of the irradiance constraint based on ground-based optical spectral measurements of the target.

2. IRRADIANCE DUE TO A SPHERICAL LAMBERTIAN SOURCE

First, some definitions. The radiant flux Φ (W) is related to radiance L (W/sr/m^2) by [1]

$$\Phi = \iint L \cos\theta dA d\omega. \tag{1}$$

To compute the radiant flux Φ arriving at a given surface A, for each area element dA we integrate over the entire solid angle ω subtended by the source. To account for the orientation of the surface relative to the incident light, we must integrate over the projected surface element $dA\cos\theta$ where θ defines the angle between the surface normal and the solid angle direction. For convenience, we may equivalently express (1) in terms of the projected solid angle $d\Omega = \cos\theta d\omega$ as described in subsection A.2 according to

$$\Phi = \iint L dA d\Omega. \tag{2}$$

The irradiance E (W/m^2) incident on a given surface element can be obtained by integrating the radiance over the projected solid angle of a hemisphere centered on the surface element

$$E = \int_{\Omega_{hemi}} L\cos\theta d\omega = \int_{\Omega_{hemi}} L d\Omega. \tag{3}$$

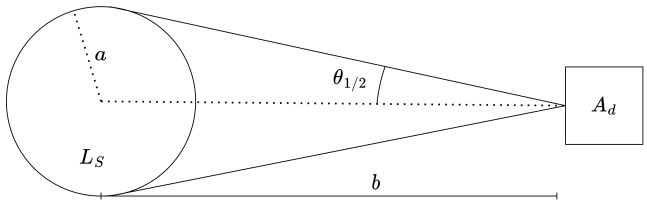

Fig. 1: Trigonometry of a Lambertian sphere and a detector of area A_d.

Now, given a sensor-target-source system, to compute the irradiance arriving at the target, we model the source after the sun and represent it as a Lambertian sphere (Figure 1). A Lambertian source is characterized by having a constant radiance, $L(\theta, \phi) = const$. From (3), we can obtain the on-axis irradiance $E_{on\text{-}axis}$ incident to the target surface due to the spherical Lambertian source by integrating over the right circular cone (see subsection A.1) of half-angle $\theta_{1/2}$

$$E_{on\text{-}axis} = \int_{\Omega_{cone}} L_{sun} \cos\theta d\omega \tag{4}$$

$$= L_{sun} \int_0^{2\pi} d\phi \int_0^{\theta_{1/2}} \sin\theta \cos\theta d\theta \tag{5}$$

$$= L_{sun} \pi \sin^2 \theta_{1/2}. \tag{6}$$

For a target surface with normal $\mathbf{n}$ that may lie off the cone axis, the total irradiance received at the surface is approximated by scaling the on-axis contribution by the dot product of the surface normal $\mathbf{n}$ and central cone axis $\hat{\omega}_i$

$$E_{sun} = (\hat{\omega}_i \cdot \mathbf{n}) E_{on\text{-}axis} = L_{sun} \pi \sin^2 \theta_{1/2} (\hat{\omega}_i \cdot \mathbf{n}). \tag{7}$$

For a spherical source of radius a with a center lying a distance b from the target surface as shown in Figure 1, we have

$$\sin^2 \theta_{1/2} = \frac{a^2}{a^2 + b^2}, \tag{8}$$

which allows us to simplify (7) as

$$E_{sun} = L_{sun} \pi \left(\frac{a^2}{a^2 + b^2} \right) \hat{\omega}_i \cdot \mathbf{n}. \tag{9}$$

For $b \gg a$, the sphere approaches a point source and we may relate the radiance of the source to the intensity I (W/sr) of a point source through $I = LA_{proj} = L\pi a^2$ [2] to thus recover the familiar inverse-square behavior of irradiance

$$E_{sun} = \frac{I_{sun}}{b^2} \hat{\omega}_i \cdot \mathbf{n}. \tag{10}$$

Given $a = r_{sun} = 6.957 \times 10^8$ m and $b = 1$ au $= 1.496 \times 10^{11}$ m, the half-angular size of the sun relative to Earth or target is approximately $\theta_{1/2} = 0.266°$ and the overestimate of $\sin^2 \theta_{1/2}$ arising from the point-source approximation is

$$E_{sun\text{-}point} / E_{sun\text{-}finite} = 1 + 2 \times 10^{-5}. \tag{11}$$

3. THE RENDERING EQUATION

The rendering equation describes the output radiance measured in the direction $\hat{\omega}_o$ and is given as [3]

$$L_o(\hat{\omega}_o, \lambda, t) = L_e(\hat{\omega}_o, \lambda, t) + \int_{\Omega_{hemi}} f(\hat{\omega}_i', \hat{\omega}_o, \lambda, t) L_i(\omega_i', \lambda, t) (\hat{\omega}_i' \cdot \mathbf{n}) d\omega_i'. \tag{12}$$

Here we integrate over a hemisphere centered around the target surface area with normal $\mathbf{n}$, adding the contributions of all incident radiance modulated by the bidirectional reflectance distribution function $f(\hat{\omega}_i', \hat{\omega}_o, \lambda)$ and projected by

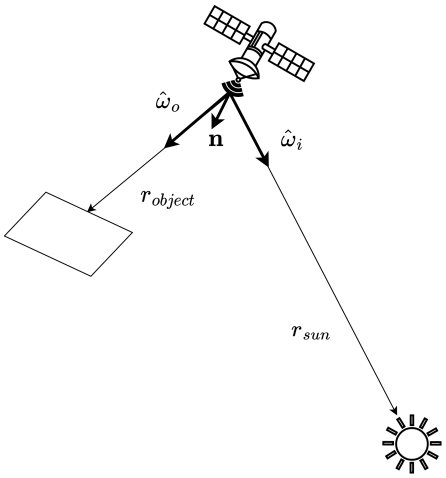

Fig. 2: Illumination geometry. For a fixed $\mathbf{n}$, the geometry may be specified by the pair of unit vectors $(\hat{\omega}_i, \hat{\omega}_o)$.

$\hat{\omega}_i' \cdot \mathbf{n}$. Radiance that is emitted by the target (i.e., thermal radiation) is represented by $L_e(\hat{\omega}_o, \lambda, t)$, which we will take to be zero.

From (3), we may use the form

$$dE = L \cos\theta d\hat{\omega} \tag{13}$$

to express the outgoing radiance as an integral over all sources of irradiance within the hemisphere reaching the target surface

$$\int_{\Omega_{hemi}} f(\hat{\omega}_i', \hat{\omega}_o, \lambda, t) L_i(\omega_i', \lambda, t)(\hat{\omega}_i' \cdot \mathbf{n}) d\omega_i' = \int_{\Omega_{hemi}} f(\hat{\omega}_i', \hat{\omega}_o, \lambda, t) dE. \tag{14}$$

With our source (sun) modeled as a point source, the incident irradiance is entirely attributed to the radiance lying along the direction $\hat{\omega}_i$ and, by substitution of (10), can be expressed as

$$dE = (\hat{\omega}_i' \cdot \mathbf{n}) \delta(\hat{\omega}_i - \hat{\omega}_i') \frac{I_{sun}}{b^2} d\hat{\omega}_i'. \tag{15}$$

Finally, substituting this into our integral of (14), we obtain the outgoing radiance in direction $\hat{\omega}_o$ due to a point-source in direction $\hat{\omega}_i$

$$L_o(\hat{\omega}_o, \lambda, t) = \int f(\hat{\omega}_i', \hat{\omega}_o, \lambda, t)(\hat{\omega}_i' \cdot \mathbf{n}) \delta(\hat{\omega}_i - \hat{\omega}_i') \frac{I_{sun}}{b^2} d\hat{\omega}_i' \tag{16}$$

$$= f(\hat{\omega}_i, \hat{\omega}_o, \lambda, t) \frac{I_{sun}(\lambda)}{b^2} (\hat{\omega}_i \cdot \mathbf{n}). \tag{17}$$

4. THE CAMERA EQUATION

The camera equation describes image irradiance at the focal plane for a basic optical system operating at finite conjugates. Let r_{image} and r_{object} represent the distance from the lens to the focal plane and object plane respectively. Let us define an optical system with effective focal length f and aperture diameter D. The magnification m is

$$m = \frac{r_{image}}{r_{object}}. \tag{18}$$

For an object at infinity, $m = 0$ and for equal conjugates, $m = 1$. The irradiance at the focal plane arising from the reflected target radiance L_o is given by [2]

$$E_{image} = \frac{\pi}{4} L_o \frac{D^2}{f^2(1+m)^2} = \frac{\pi}{4} L_o \left(\frac{D}{f}\right)^2 \frac{r_{object}^2}{(r_{object} + r_{image})^2}. \tag{19}$$

Given the outgoing radiance of (17) along direction $\hat{\omega}_o$ and given $r_{object} \gg r_{image}$, the image-plane irradiance may be simplified as

$$E_{image}(\lambda, t) = \frac{\pi}{4}\left(\frac{D}{f}\right)^2 \frac{I_{sun}(\lambda)}{r_{sun}^2} f(\hat{\omega}_i, \hat{\omega}_o, \lambda, t)(\hat{\omega}_i \cdot \mathbf{n}). \tag{20}$$

Note that the focal plane lies in the direction of $-\hat{\omega}_o$.

From (20) we see that the irradiance at the image plane scales as $1/r^2$ for the source-to-target distance and that the total irradiance received is scaled by the cosine of the angle between the source and target normal. For imaging areas that deviate from the optical axis and subtend an angle α, it is worth noting that the irradiance scales as $\cos^4 \alpha$. Given the 0.05 arcsec angular diameter of a 10 m target, the error in irradiance from neglecting the cosine falloff is approximately

$$E_{image}/E_{extended\text{-}image} = 1 + 1.55 \times 10^{-13}. \tag{21}$$

The mapping between image-plane irradiance and pixel intensities is non-linear. The number of electrons generated per unit area in the photodetector may be roughly estimated as

$$N_{electron}(\lambda) = E_{image}(\lambda, t)\left(\frac{\lambda}{hc}\right) \times \text{Quantum Efficiency} \times \Delta t \times \text{Camera Gain}. \tag{22}$$

The amplified electron count undergoes analog signal processing and ADC quantization to finally arrive at pixel intensity. While a sharper model of the detection stage can be constructed, it is not needed for our purposes here.

5. THE HELMHOLTZ RECIPROCITY CONSTRAINT

Let us first simplify our expression for the irradiance received at the image plane, (20). Given the small eccentricity of Earth's orbit, we take $\frac{dr_{sun}}{dt} = 0$. Given that the solar intensity is, to a decent approximation, constant over time we take $\frac{dI_{sun}}{dt} = 0$. It then follows that

$$E_0 \equiv \frac{\pi}{4}\left(\frac{D}{f}\right)^2 \frac{I_{sun}(\lambda)}{r_{sun}^2} = const. \tag{23}$$

Here E_0 is a strictly theoretical quantity representing a maximal received irradiance in which all incident energy within the solid angle subtended by the source is reflected by the target and received at the detector. With E_0 we may then express the irradiance at the image plane as

$$E_{image}(\hat{\omega}_i, \hat{\omega}_o, \lambda, t) = E_0 f(\hat{\omega}_i, \hat{\omega}_o, \lambda, t)(\hat{\omega}_i \cdot \mathbf{n}). \tag{24}$$

The BRDF f is constrained to obey the following properties:

$$f(\hat{\omega}_i, \hat{\omega}_o) \geq 0 \qquad \text{(positivity)} \tag{25}$$

$$f(\hat{\omega}_i, \hat{\omega}_o) = f(\hat{\omega}_o, \hat{\omega}_i) \qquad \text{(Helmholtz reciprocity)} \tag{26}$$

$$\forall \hat{\omega}_i, \int_{\Omega_{hemi}} f(\hat{\omega}_i, \hat{\omega}_o)(\hat{\omega}_o \cdot \mathbf{n}) d\hat{\omega}_o \leq 1 \qquad \text{(energy conservation)} \tag{27}$$

Helmholtz reciprocity can be derived from the basis of time-reversal symmetry associated with the Maxwell field equations. Simply put, the reciprocity states that if we exchange the locations of the source and detector, the BDRF will remain invariant.

We can make use of such a principle to derive a constraint that relates the irradiances measured between two conjugate points as shown in Figure 3. The illumination geometry of the source-target-sensor system is specified by the ordered pair of unit-vector directions, (source, sensor). Given $(\text{source}, \text{sensor}) = (\hat{\omega}_1, \hat{\omega}_2)$, the irradiance E_{12} at the image plane is

$$E_{12}(\lambda) = E_0 f(\hat{\omega}_1, \hat{\omega}_2, \lambda, t)(\hat{\omega}_1 \cdot \mathbf{n}). \tag{28}$$

For the conjugate geometry, the illumination geometry is $(\text{source}, \text{sensor}) = (\hat{\omega}_2, \hat{\omega}_1)$ and the irradiance E_{21} on the image plane is

$$E_{21}(\lambda) = E_0 f(\hat{\omega}_2, \hat{\omega}_1, \lambda, t)(\hat{\omega}_2 \cdot \mathbf{n}). \tag{29}$$

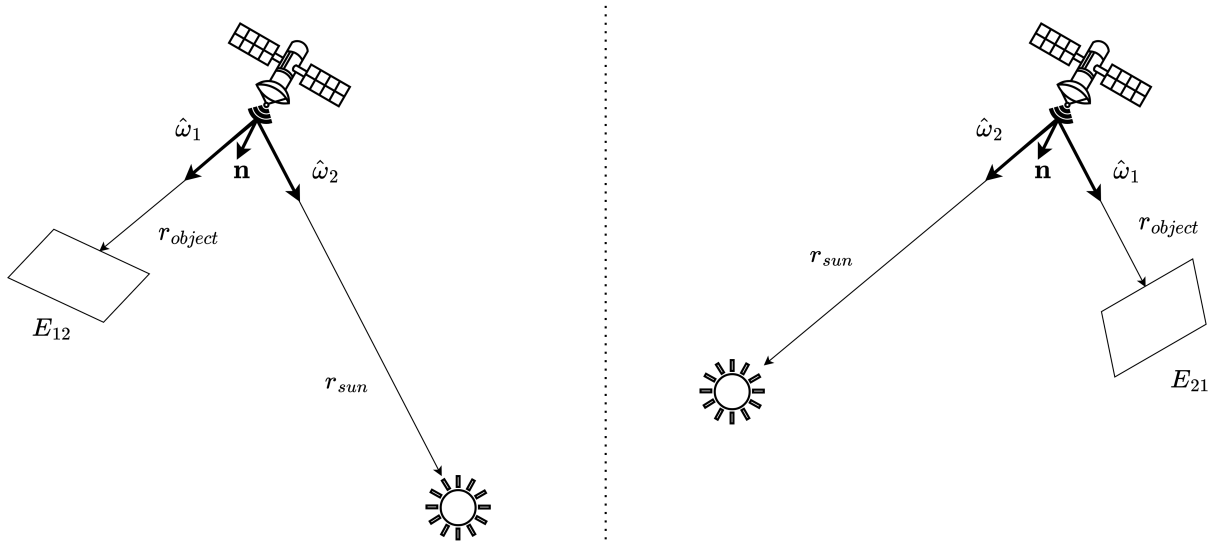

Fig. 3: Two conjugate geometries, obtained by $(\hat{\omega}_1, \hat{\omega}_2) \longleftrightarrow (\hat{\omega}_2, \hat{\omega}_1)$. Note that the orientation of the target differs in the image plane of each conjugate system, while the BRDF remains invariant.

Solving for the BRDF, Helmholtz reciprocity leads to the equality

$$\frac{E_{12}(\lambda)}{E_0(\hat{\omega}_1 \cdot \mathbf{n})} = \frac{E_{21}(\lambda)}{E_0(\hat{\omega}_2 \cdot \mathbf{n})}. \tag{30}$$

This can be simplified into a constraint relating measured irradiances E_{12} and E_{21}, target surface normal $\mathbf{n}$, and direction vectors $\hat{\omega}_1$ and $\hat{\omega}_2$ as

$$(E_{12}(\lambda)\hat{\omega}_2 - E_{21}(\lambda)\hat{\omega}_1) \cdot \mathbf{n} = 0. \tag{31}$$

6. APPLICATION

For resident space objects in a geostationary orbit – an assumption that can be relaxed but would require a more involved treatment – let us assume that a large baseline of optical measurements of a nadir-pointing satellite can be obtained over a wide variety of illumination geometries. Over a 24-hour period, the incident direction vector of the sun $\hat{\omega}_i$ sweeps a continuous semi-circle path of illumination directions that lie within our observation window. On an annual timescale, the inclination of the orbital plane of the sun (in a reference frame inertial to the target) continuously increases and then decreases (i.e., seasonal variation), resulting in an appreciable subset of the BRDF unit-sphere that is able to be sampled by ground-based sensors. While one could elect to utilize single band photometric measurements as the basis for optical observations, we are encouraged by the use of past works [4][5] which demonstrate that high-resolution spectra provide a rich source of information related to a satellite's unique material composition, geometry, and orientation.

Given such a baseline, the Helmholtz reciprocity constraint of (31) allows us to relate the irradiance of a) a target that has changed its pointing angle to $\mathbf{n} + \Delta\mathbf{n}$ to b) a pre-registered target with pointing angle $\mathbf{n}$ that coincides with its conjugate geometry. This is most easily visualized through Figure 3 which illustrates that the orientation of the target as measured by E_{12} differs from its orientation at the conjugate point measured by E_{21}.

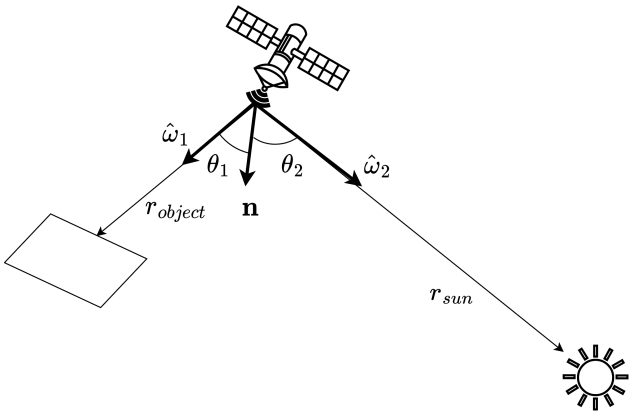

Fig. 4: Illumination geometry in terms of angles θ_1 and θ_2.

The ratio between the two conjugate irradiances themselves differs by an overall scalar factor. In reference to Figure 4, we can express the Helmholtz reciprocity constraint of (31) in terms of the angles θ_1 and θ_2 as

$$E_{12}(\lambda)\cos\theta_2 = E_{21}(\lambda)\cos\theta_1 \tag{32}$$

or

$$\frac{E_{12}(\lambda)}{E_{21}(\lambda)} = \frac{\cos\theta_1}{\cos\theta_2}. \tag{33}$$

In sum, to a first order approximation the irradiances associated with two conjugate geometries are directly proportional to each other over the full set of wavelengths sampled. Interestingly, the Helmholtz reciprocity relation also implies that there are clear degeneracies associated with inferring a target's orientation from optical spectra under real illumination geometries.

7. ASSUMPTIONS

- The Sun is a Lambertian sphere: Given the sun is *almost* a perfect blackbody radiator, the errors due to this assumption are going to be very small. That said, the sun does possess non-uniform radiance, temperature variations, spectral variations, and surface features.
- The Sun may be treated as a point source: As shown in (11), the irradiance error associated with the finite radius of the Sun is given as $E_{sun\text{-}point}/E_{sun\text{-}finite} = 1 + 2 \times 10^{-5}$.
- The target may be treated as a point source: For a geosynchronous object of 10 m in diameter, the angular diameter as seen from an Earth sensor is approximately 0.05 arcsec. Computing the difference in irradiance in the same manner as the Sun, we find an error on the order of $E_{target\text{-}point}/E_{target\text{-}finite} = 1 + 10^{-14}$. (Intuitively, the Sun occupies a much larger angular extent than a geosynchronous satellite in the sky, so this seems reasonable). In addition, the contribution of the $\cos^4\alpha$ falloff associated with a finite angular extent of the target is approximately $E_{image}/E_{extended\text{-}image} = 1 + 1.55 \times 10^{-13}$.
- The off-axis irradiance can be computed from the on-axis radiance by simply scaling it by the dot product $\hat{\omega}_i \cdot \mathbf{n}$. Such an approximation is not uncommon and one may refer to its role in Lambert's cosine law. Given the differential area element associated with the irradiance, the approximation is reasonable. To compute the off-axis correction directly, one needs to set up and compute an integral over a tilted right circular cone. Once the coordinate system and proper bounds of integration are determined, such a computation is likely to require numerical integration.
- The optical system is simple and ideal, admitting perfect optical and atmospheric transmittance.

- No atmosphere: The underlying assumption here is that the *dispersive* effects of the atmosphere (absorption, transmission, reflection) have little statistical variation over the observation time windows.
- The target can be modeled as a single surface with normal $\mathbf{n}$: Since the target is modeled as a point source, we let $\mathbf{n}$ represent the mean surface normal $\langle \mathbf{n} \rangle$ and associate with it a spatially averaged BRDF. As we depart from this assumption, we must give up analytical tractability and pivot towards a full-scale simulation with micro-faceted BRDFs. Another confounding detail not present in this assumption is that, for satellites, solar panels articulate. We expect this to pose a formidable, but not impossible challenge. Fortunately, we can estimate the rotation angle of solar panels with a very high likelihood. Decoupling the effects of panel articulation from bus pointing angle may be slated for higher order corrections in future-future work.
- No thermal emission: Thermal radiation, especially from the large surface area of satellite solar panels is not insignificant. However, this radiation primarily lies in the NIR or larger wavelengths. For optical spectra $\lesssim 1000$ nm, we expect thermal radiation to be negligible.
- $f(\hat{\omega}_1, \hat{\omega}_2, \lambda, t) = f(\hat{\omega}_2, \hat{\omega}_1, \lambda, \tau)$: While Maxwell's equations show this holds for $t = \tau$, we have implicitly made the assumption that the BRDF is approximately the same at conjugate times t and τ. Given that we have modeled the target as a point source with a spatially averaged BRDF, we expect the variance in the BRDF at two conjugate times to be small given a sufficiently small $\Delta t = |t - \tau|$. What is sufficiently small? One metric for this is the time scale by which materials start to significantly deviate due to space aging. The time difference assumption here in general falls within the same vein of work regarding spectral concept drift [6].

8. RELATED WORK

The first paper proposing the notion of the BRDF was in 1965 [3]. Since its inception, there have indeed been other works that attempt to exploit Helmholtz reciprocity [7][8][9] for imaging applications. These works lie in the domain of classical computer vision at the intersection of geometric stereo and photometry. They concern natural resolved imaging and comprise experiments where the illumination source and camera are precisely positioned and controlled. In these works, a sequence of conjugate observations allows one to stack the constraints of (31) into a matrix by which one can use singular-value-decomposition or least squares optimization to make an estimate of the normal vector $\mathbf{n}$ and depth at each pixel in the image. The results are compelling as seen in Figure 5 referenced from [8]. However, such a technique's utility may ultimately be limited by the need to precisely measure or control the system geometry of the sensor-target-source positioning. Such methods should be contrasted with recent developments in neural radiance fields that are independent of both camera intrinsics and extrinsics [10]. For the space domain, the relative positioning between the sensor, target, and source is precisely defined via astrodynamical propagators and thereby may prove to be a well-suited candidate for leveraging Helmholtz reciprocity.

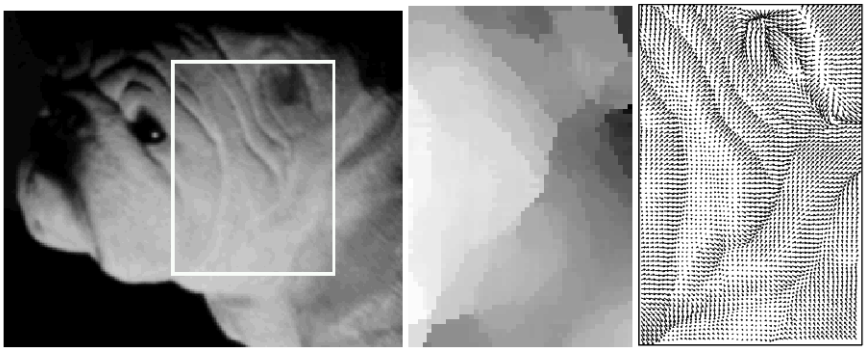

Fig. 5: A reconstruction of the marked interior region (a) of a ceramic figurine. Figures (b) and (c) are the depth map and the quiver plot of the normal field. The low resolution of the depth map is caused by the 11 × 11 window used in the depth search, but this does not affect the accuracy of the estimated normal field. 18 reciprocal image pairs were used.

REFERENCES

[1] Frank L Pedrotti, Leno M Pedrotti, and Leno S Pedrotti. *Introduction to optics*. Cambridge University Press, 2017.

[2] James M. Palmer and Barbara G. Grant. *The art of radiometry*. OCLC: ocn437115790. Bellingham, Wash: SPIE Press, 2010. 369 pp. ISBN: 978-0-8194-7245-8.

[3] Fred E Nicodemus. "Directional reflectance and emissivity of an opaque surface". In: *Applied optics* 4.7 (1965), pp. 767–775.

[4] Matthew Phelps et al. "SPECTRANET-SO(3): Learning Satellite Orientation from Optical Spectra by Implicitly Modeling Mutually Exclusive Probability Distributions on The Rotation Manifold". In: *ICASSP 2023 - 2023 IEEE International Conference on Acoustics, Speech and Signal Processing (ICASSP)*. 2023, pp. 1–5. DOI: 10.1109/ICASSP49357.2023.10095921.

[5] J Zachary Gazak et al. "SpectraNet: Learned Recognition of Artificial Satellites from High Contrast Spectroscopic Imagery". In: *Proceedings of the IEEE/CVF Winter Conference on Applications of Computer Vision*. 2022, pp. 4012–4020.

[6] J Zachary Gazak et al. "Model validity dynamics in learned spectroscopic recognition of satellites". In: *Algorithms, Technologies, and Applications for Multispectral and Hyperspectral Imaging XXIX*. Vol. 12519. SPIE. 2023, pp. 58–68.

[7] Peter Tu et al. "Surface registration with a Helmholtz reciprocity image pair". In: *IEEE Workshop on Color and Photometric Methods in Computer Vision*. Vol. 7. 2003.

[8] Todd Zickler, Peter N. Belhumeur, and David J. Kriegman. "Helmholtz Stereopsis: Exploiting Reciprocity for Surface Reconstruction". In: *Computer Vision — ECCV 2002*. Ed. by Anders Heyden et al. Red. by Gerhard Goos, Juris Hartmanis, and Jan van Leeuwen. Vol. 2352. Series Title: Lecture Notes in Computer Science. Berlin, Heidelberg: Springer Berlin Heidelberg, 2002, pp. 869–884. ISBN: 978-3-540-43746-8 978-3-540-47977-2. DOI: 10.1007/3-540-47977-5_57. URL: http://link.springer.com/10.1007/3-540-47977-5_57 (visited on 03/14/2023).

[9] S. Magda et al. "Beyond Lambert: reconstructing surfaces with arbitrary BRDFs". In: *Proceedings Eighth IEEE International Conference on Computer Vision. ICCV 2001*. Eighth IEEE International Conference on Computer Vision. Vol. 2. Vancouver, BC, Canada: IEEE Comput. Soc, 2001, pp. 391–398. ISBN: 978-0-7695-1143-6. DOI: 10.1109/ICCV.2001.937652. URL: http://ieeexplore.ieee.org/document/937652/ (visited on 04/05/2023).

[10] Zirui Wang et al. "NeRF–: Neural radiance fields without known camera parameters". In: *arXiv preprint arXiv:2102.07064* (2021).

A. APPENDIX

A.1 Right Circular Cones

Given that most optical systems have circular apertures, rather than using the canonical solid angle defined by

$$\omega = \iint \sin\theta d\theta d\phi \tag{34}$$

which represents the solid angle subtended by a curvilinear square-like patch on the unit sphere (due to $d\theta$ and $\sin\theta d\phi$ being orthogonal), it is helpful to use the solid angle associated with a right circular cone parametrized by half angle $\theta_{1/2}$ as shown in Figure 6

$$\omega = \int_0^{2\pi} d\phi \int_0^{\theta_{1/2}} \sin\theta d\theta = 2\pi(1-\cos\theta_{1/2}) = 4\pi\sin^2\left(\frac{\theta_{1/2}}{2}\right). \tag{35}$$

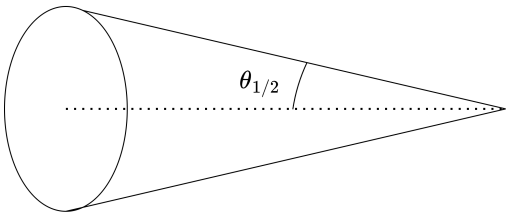

Fig. 6: Right circular cone of half-angle $\theta_{1/2}$.

A.2 Projected Solid Angles

Given that radiance is defined as the flux per unit solid angle *per unit projected area*, it is helpful to define a quantity related to the area subtended by a solid angle that is projected onto the plane of the observer as shown in Figure 7. To differentiate from the canonical solid angle ω, we denote the projected solid angle as Ω and define it as

$$d\Omega = \sin\theta \cos\theta d\theta d\phi. \tag{36}$$

Solid angle and projected solid angle are related as

$$d\Omega = \cos\theta d\omega. \tag{37}$$

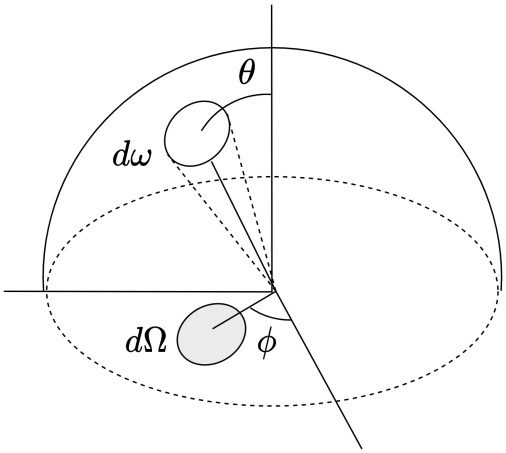

Fig. 7: Projected solid angle Ω.

For small solid angles, we can approximate the projected solid angle as $\Omega = \omega \cos\theta$. However, for large solid angles, we must integrate over $\cos\theta$ for each differential area to compute the correct projected area. For the hemisphere, $\omega = 2\pi$ while $\Omega = \pi$.

The projected solid angle associated with a right circular cone can be computed as

$$\Omega = \int_0^{2\pi} d\phi \int_0^{\theta_{1/2}} \sin\theta \cos\theta d\theta = \pi \sin^2\theta_{1/2}. \tag{38}$$